THz mixing of high-order harmonics using YBa2Cu3O7−δ nanobridges

Applied Physics Letters

RESEARCH ARTICLE | FEBRUARY 24 2026

THz mixing of high-order harmonics using $YBa_2Cu_3O_{7-\delta}$ nanobridges

Núria Alcalde-Herraiz ; Alessia Garibaldi ; Karn Rongrueangkul ; Alexei Kalaboukhov ; Floriana Lombardi ; Sergey Cherednichenko ; Thilo Bauch

Appl. Phys. Lett. 128, 082601 (2026)
https://doi.org/10.1063/5.0309494

AIP Publishing

Applied Physics Letters ARTICLE pubs.aip.org/aip/apl

THz mixing of high-order harmonics using $YBa_2Cu_3O_{7-\delta}$ nanobridges

Cite as: Appl. Phys. Lett. **128**, 082601 (2026); doi: 10.1063/5.0309494
Submitted: 28 October 2025 · Accepted: 3 February 2026 ·
Published Online: 24 February 2026

Núria Alcalde-Herraiz,[1,a)] Alessia Garibaldi,[1,2] Karn Rongrueangkul,[1] Alexei Kalaboukhov,[1] Floriana Lombardi,[1] Sergey Cherednichenko,[3] and Thilo Bauch[1,b)]

AFFILIATIONS

[1]Quantum Device Physics Laboratory, Department of Microtechnology and Nanoscience, Chalmers University of Technology, Gothenburg, Sweden
[2]Department of Clinical Neuroscience, Institute of Neuroscience and Physiology, University of Gothenburg, Gothenburg, Sweden
[3]Terahertz and Millimeter Wave Laboratory, Department of Microtechnology and Nanoscience, Chalmers University of Technology, Gothenburg, Sweden

[a)]**Author to whom correspondence should be addressed:** herraiz@chalmers.se
[b)]**Electronic mail:** thilo.bauch@chalmers.se

ABSTRACT

Superconducting materials are key for technologies enabling a large number of devices, including THz wave mixers and single-photon detectors, though they are limited at very low temperatures for conventional superconductors. High-temperature operation could, in principle, be offered using cuprate superconductors. However, the complexity of the material in thin film form, the extremely short coherence length, and material stability have hindered the realization of THz devices working at liquid nitrogen temperatures. $YBa_2Cu_3O_{7-\delta}$ (YBCO) nanodevices have demonstrated nonlinear properties typical of Josephson-like behavior, which have the potential for mixing of AC signals in the THz range due to the large superconducting energy gap. Here, we present AC Josephson functionalities for terahertz waves utilizing Abrikosov vortex motion in nanoscale-confined, fully planar YBCO thin film bridges. We observe Shapiro step-like features in the current–voltage characteristics when irradiating the device with monochromatic subterahertz waves (100–215 GHz) at 77 K. We further explore these nonlinear effects by detecting THz high-order harmonic mixing for signals from 200 GHz up to 1.4 THz using a local oscillator at 100 GHz. Our results open a path to an easily fabricated HTS nonlinear nanodevice based on dimensional confinement, suitable for terahertz applications.

Photodetection in the terahertz (THz) frequency range ($f \approx 0.1$–10 THz)[1–3] is essential in emerging technologies in imaging,[4] spectroscopy,[5] and quantum information.[6] Despite considerable progress in semiconducting devices, superconductors are vital in bridging this frequency range when high sensitivity, high frequency, or large pixel-count imaging are of concern.[7,8] Here, typical implementations are transition-edge sensors, hot-electron bolometers, Josephson junctions, and kinetic inductance detectors, to name a few. However, most implementations rely on low-temperature superconductors (LTS), requiring cryogenic cooling from 4 to 20 K, which significantly limits practical operation.

Implementing devices with critical temperature (T_C) above 20 K would alleviate the requirement of costly cryogenic cooling equipment. Here, for example, MgB_2 with a T_C slightly below 40 K has been used for THz and IR detectors.[9,10] Instead, high-temperature superconductor (HTS) devices, such as those based on $YBa_2Cu_3O_{7-\delta}$ (YBCO), offer a compelling alternative by enabling, in principle, operation at liquid nitrogen temperatures achievable with simple and low-cost cryo-coolers. State-of-the-art HTS harmonic mixers employ the nonlinear current phase relation (CPR) of Josephson Junctions (JJs) realized using different techniques like bicrystal,[11,12] step-edge,[13,14] and oxygen ion-irradiation.[15,16] However, for these devices, the range of operation remains restricted to subterahertz frequencies. Higher frequency values (up to 640 GHz) are achieved at temperatures below 20 K,[17] and similarly, devices based on HTS $Bi_2Sr_2CaCu_2O_{8+x}$ intrinsic JJs report mixing at frequencies up to 1.6 THz at 6 K.[18–20]

While most superconducting mixers rely on barrier-based JJs, there is a growing interest in replacing the active element with a simple superconducting constriction that does not contain any barrier. This mitigates fabrication complexity and could avoid detrimental effects

due to barrier imperfections.[21,22] Indeed, nonlinear CPR is not limited to conventional barrier-based Josephson Junctions. Dayem bridges[23] offer a scalable route to Josephson-like behavior by nanopatterning a constriction in a bare film.[24] Their transport properties, governed by geometrical confinement,[23,25] allow Josephson-like dynamics even when the bridge length exceeds the coherence length ($l \gg \xi_0$), provided the width is below the Pearl length ($w \ll \lambda_L^2 t^{-1}$, where t is the film thickness, and λ_L is the London penetration depth). In this limit, the Josephson-like behavior is enabled through coherent Abrikosov vortex dynamics.[24] Such structures have explored the physics of non-equilibrium superconductivity[26–30] and inspired the development of novel superconducting nanodevices.[31–34]

Here, we demonstrate THz harmonic mixing in YBCO Dayem nanobridges integrated with planar antennas, operating at temperatures up to 77 K. In these devices, the finite voltage state is determined by vortex dynamics. Harmonic mixing up to 1.4 THz (14th harmonic) is achieved, with the upper frequency limit set by the RF source and measurement setup rather than by intrinsic device constraints. These findings establish YBCO nanobridges as a promising technology for high-frequency THz detection enabled by coherent Abrikosov dynamics.

The HTS devices were fabricated from 50 nm-thick overdoped, untwinned YBCO films grown on (110)-oriented MgO substrates.[35] The device layout consists of a YBCO spiral antenna with an embedded bridge, as shown in a false-color scanning electron microscope (SEM) image in Fig. 1(a). Each nanobridge had widths (w) and lengths (l) of 70×50 and 200×400 nm^2, see the inset in Fig. 1(a). The devices were patterned by a single-step lithography process combining a carbon mask, electron beam lithography, and Ar ion beam etching[36] (see supplementary material Note 1). This nanofabrication process preserves the superconducting properties of the YBCO film, yielding highly reproducible devices with critical current densities approaching the theoretical depairing limit.[37] In addition, transmission electron microscope imaging[38] and noise[39] measurements demonstrate that our nanobridges do not contain any grain boundaries, further confirming the uniformity of the fabricated devices. Electrical characterization of our devices was performed in a two-point contact configuration in a DynaCool Physical Properties Measurement System (Quantum Design Inc., USA), which yielded a superconducting critical temperature of $T_C = 84.8$ K, Fig. 1(b), comparable to previously reported overdoped, untwinned 50 nm-thick films.[40] Furthermore, given the critical current density at 77 K being 1.2×10^6 Acm^{-2} extrapolation from the Bardeen expression $J_C \propto (1 - (T/T_C)^2)^{3/2}$[41] would give a value of $\sim 2 \times 10^7$ Acm^{-2} at temperatures below 4 K, comparable to our previously reported data.[37]

The devices were characterized by mixing THz signals up to 1.4 THz in the setup illustrated in Fig. 1(c), see also supplementary material Note 1 for more details. In this configuration, it was possible to obtain both the current–voltage characteristics (IVCs) and the intermediate frequency output power of the device as a function of the voltage across the device when using it as a heterodyne mixer.

In the absence of illumination, the IVCs of the nanobridges vary across the studied temperature range, as shown in Fig. 2(a) for the 70×50 nm^2 bridge, and which is representative of the wider geometry as discussed in supplementary material Note 2. Increasing the temperature both reduces the critical current and alters the shape of the finite-voltage branch in the IVC. At 60 K, a flux-flow (FF) voltage state, characterized by a downward curvature in the IVC[42] and indicative of vortex dynamics, is observed in the current range $I_C < I < 605\ \mu$A reaching a maximum voltage of 6 mV [highlighted as gray zone in Fig. 2(a)]. After this voltage, a flux-flow instability occurs, followed by the resistive state with a stable hotspot ($V > 30$ mV).[43] It is interesting to note that many studies performed on LTS bridges reveal that the FF regime is only accessible for $T \lesssim T_C$ or under a magnetic field.[29,44] In

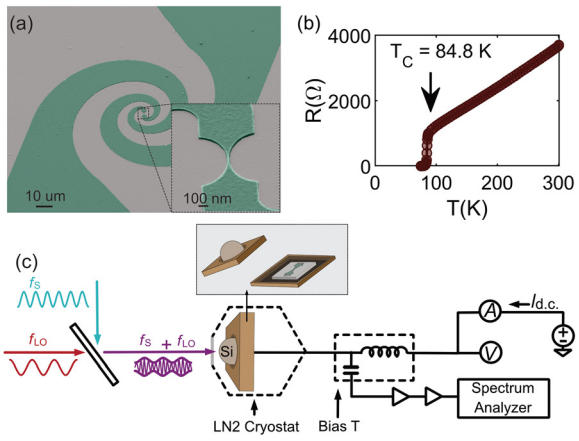

FIG. 1. Design and characterization of nanobridge heterodyne detectors and measurement setup. (a) SEM false-color image of a 70 nm wide YBCO nanowire integrated with a YBCO spiral antenna on a MgO substrate. The inset shows a zoom-in of the nanowire oriented along the *a*-axis. (b) Resistance as a function of the temperature of the device. (c) Schematic of the measurement setup with an inset showing the device inside the sample box (see supplementary material Note 1 for more details).

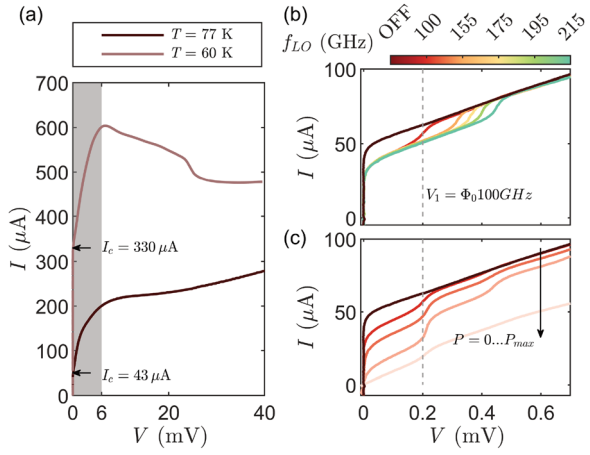

FIG. 2. Photo-induced response of a bridge with a cross section of 70×50 nm^2. (a) IVCs for a nanobridge for temperatures 77 and 60 K where the critical currents are indicated for both curves. (b) Measurement at 77 K of the current–voltage characteristic without an applied signal and with an applied frequency $f_{LO} = 100$, 155, 175, 195, and 215 GHz. (c) Evolution at 77 K of the current–voltage characteristic for the non-illumination case and for increasing illumination power at $f_{LO} = 100$ GHz.

contrast, in YBCO nanobridges, the FF regime expands to a broader range of temperatures and does not require an externally applied magnetic field.[37,42,45]

The nanobridge exhibits Shapiro-like current steps in the FF region, which are analogous to the ones observed in conventional JJs,[46] when illuminated with RF signals in the range of 100–215 GHz, even at 77 K, see Fig. 2(b). In the case of a bridge, these steps in the IVCs are due to phase-locking the radiation frequency to the coherent motion of Abrikosov vortices and appear at specific voltages V_n given by the relation $V_n = nf_{LO}\Phi_0$, where V_n is the voltage at the integer step number n, Φ_0 is the magnetic flux quantum, and f_{LO} is the frequency of the external LO, see Fig. 2(b).[25,47] Observation of Shapiro steps in the nanobridge required its width to be smaller than the Pearl length λ_P. This is the case for our devices, considering a film thickness of $t = 50$ nm and previously reported London penetration depths in similar devices in a range from 270 to 350 nm.[48,49] While Shapiro-like steps have been observed in Dayem bridges under microwave irradiation (1 GHz to 20 GHz) at low temperatures (around 4 K),[45,50] this work demonstrates such steps at frequencies above 100 GHz at 77 K. The observation of Shapiro-like steps indicates coherent Abrikosov dynamics in the device, which should also enable the detection of harmonic mixing.

Figure 3 shows the second harmonic mixing response of the nanobridge at $T = 77$ K and 60 K, using a LO at $f_{LO} = 100$ GHz applied together with a signal $f_S = 201$ GHz. For both temperatures, the LO power was adjusted to suppress the critical current I_C to half of its zero-power value to measure at equivalent I_{AC}/I_C, see supplementary material Note 3. Figure 3(a) (right axis) shows the amplified intermediate frequency (IF) power output from the device, P_{IF}, at $|f_S - 2f_{LO}| = 1$ GHz as a function of the DC voltage bias V across the nanobridge, with the corresponding IVC (left axis), see supplementary material Note 1 for more details. To resolve current steps at higher voltage bias, we calculated the differential resistance dV/dI, see Fig. 3(b). At both temperatures, IF power is measurable up to 2 mV, ranging from -40 dBm to -80 dBm. Remarkably, this occurs even at 77 K without any discernible Shapiro steps in the dV/dI at high voltages.

Vertical dashed lines in Figs. 3(a) and 3(b) indicate the voltage positions of the minima in dV/dI. We first note that at high voltages, the minima in dV/dI become offset relative to the minima of the IF output. Also that while the first three steps closely follow the expected dependence $V_n = nf_{LO}\Phi_0$, for $n > 3$, the spacing between Shapiro-like steps increases with increasing voltage (or n), deviating from the expected behavior. While voltage offsets between the minima in IF output power and Shapiro-step position have also been observed in JJs,[51] the origin of the deviation of these Shapiro-like steps from their expected voltage values remains unclear. Similar behavior has been reported for Josephson junctions under strong high frequency dissipation and thermal fluctuations,[52] suggesting a possible link to the dissipative nature of the vortex dynamics combined with the thermal noise. Figure 3(c) shows that at $T = 60$ K, the current steps in the IVC appear at the expected voltage values, indicating that the temperature has an effect on the vortex dynamics. This phenomenology is further illustrated in Fig. 3(e), where Lorentzian fits to the dV/dI minima in Figs. 3(b) and 3(d) yield step voltages V_n, that, when plotted against step number n, reveal a deviation from linearity at 77 K, in contrast to the linear behavior at 60 K.

To explore the harmonic mixing performance of the 70 nm wide bridge at higher frequencies, we increased f_S up to 1 THz (10th harmonic mixing). Although the IVC measured at 58 K shown in Fig. 4(a) remains comparable to that in Fig. 3(c), the resulting $P_{IF}(V)$ signal displays a weaker and aperiodically spaced minima. The microscopic origin of this behavior is not yet understood and may involve a subtle interplay between vortex dynamics and THz radiation, a matter that will be studied in future work. However, this reduced voltage dependence can also be advantageous, as it broadens the bias range over which a nearly flat IF power is maintained.

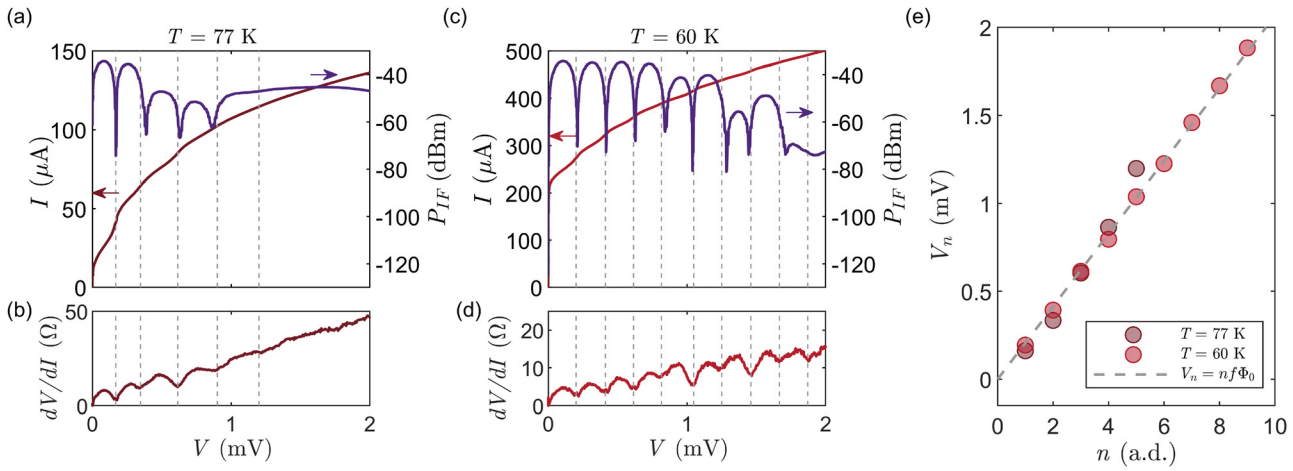

FIG. 3. Second harmonic mixing using $f_{LO} = 100$ GHz with $f_S = 201$ GHz for a bridge with a cross section of 70×50 nm^2. (a) IVC (left axis) and output power response detected at $f_{IF} = 1$ GHz (right axis) at $T = 77$ K. (b) Differential resistance obtained from IVC from panel (a) as a function of voltage. (c) IVCs measurement (left axis) and output power response (right axis) measured at temperature $T = 60$ K. (d) Differential resistance obtained from panel (c) as a function of voltage. The vertical dashed lines indicate the voltages corresponding to the minima of differential resistance. (e) Voltage position of current steps from panels (a) and (c) as a function of the step number for $T = 77$ K and $T = 60$ K, respectively. The voltage positions are obtained after fitting a Lorentzian to the corresponding minima of the differential resistance. The standard deviation of the fitting is smaller than the marker size.

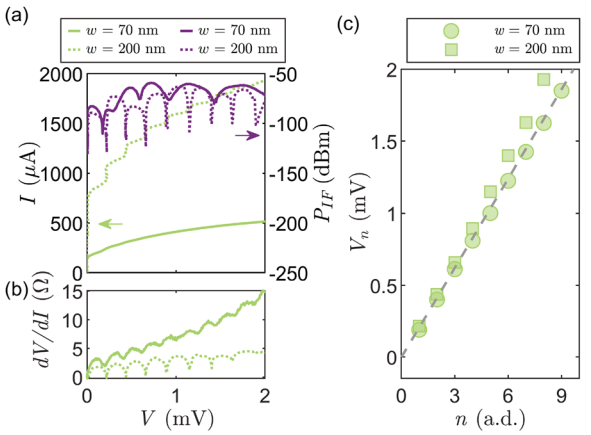

FIG. 4. Comparison of tenth harmonic mixing using $f_{LO} = 100$ GHz and $f_S = 1001$ GHz in bridges with cross sections of 70×50 nm^2 and 200×50 nm^2, biased at equivalent AC currents at temperatures $T = 59$ K and $T = 58$ K, respectively. (a) IVC measurement (left axis) and output power response detected a $f_{IF} = 1$ GHz (right axis). (b) Differential resistance dV/dI obtained from the IVCs shown in (a) as a function of voltage. (c) Voltage positions of current steps obtained from fitting a Lorentzian to the minima of the differential resistances shown in (a) and (c) as a function of the step number. The standard deviation of the fitting is smaller than the marker size.

When increasing the bridge width to 200 nm, the behavior changes. The $P_{IF}(V)$ acquires a sharper, strongly quasi-periodic modulated profile, as shown in Fig. 4(a), and the IVC curve shows more pronounced Shapiro-like current steps, similar to the ones observed for the second harmonic mixing in the 70 nm bridge in Fig. 3. Indeed, the differential resistance [Fig. 4(b)] shows that the 200 nm bridge exhibits sharper minima, consistent with better-defined steps in the IVC. However, as in the narrower bridge at 77 K, the voltage positions V_n against the step number n deviate from the linear trend, see Fig. 4(c). The deviation for the wider bridge persists even at 60 K, suggesting that temperature further modifies vortex dynamics, affecting Shapiro step positions, but not harmonic mixing. Importantly, this highlights the robustness of high-order harmonic mixing, which remains unaffected by the visibility of Shapiro steps. For devices with width exceeding the Pearl length, second harmonic mixing is still observed (see supplementary material Note 5), but at significantly lower IF power, and no visible Shapiro step in the IVCs. A comprehensive study of how bridge length and width influence device performance will be conducted in future work.

It is worth discussing the ultimate limit of harmonic mixing in YBCO nanobridge detectors, which is instrumental for device implementation. In this work, we identify two key factors limiting the mixing response: the superconducting energy gap and vortex dynamics.

A fundamental constraint is set by the superconducting energy gap of YBCO, which defines the upper voltage, and thus frequency limit for mixer operation. At 60 K, the gap corresponds to approximately 12.5 mV,[53] which would typically suggest an upper frequency limit of around 6 THz for the AC Josephson effect. However, experiments on Nb Josephson junctions have shown that, especially at low temperatures, Shapiro steps and harmonic mixing can still be observed at frequencies exceeding the superconducting gap value.[54]

A second intrinsic limitation arises from vortex dynamics in the nanobridge. As shown in Fig. 2(a), vortex dynamics should be present through the flux-flow branch, extending up to 6 mV, beyond which we observe a flux-flow instability. This behavior is further supported by Fig. 5(a), which shows the characteristic minima in the IF power response associated with Shapiro-like steps in the IVC up to 5.5 mV, indicating that vortex motion remains phase-locked to the LO even at high voltages. The onset of flux-flow instability beyond this voltage is dependent on the maximum vortex velocity achievable in our material, which is influenced by both electron diffusivity and quasiparticle relaxation rate.[26,50,55] Whether the 6 mV threshold sets a fundamental limit on the maximum signal frequency remains an open question. More studies on this phenomenology would be valuable not only for optimizing THz detection in the current devices but also for other applications where fast vortex motion is of interest. In principle, one could even extend the flux-flow region using thinner films since our preliminary investigation shows that the flux-flow regime extends up to 50 mV at 4 K in optimally doped samples.[40] Therefore, thickness and doping-dependent mixing response will be instrumental in understanding if one can push the vortex flow regime to even higher voltages.

In this study of high-order harmonic mixing in YBCO Dayem bridges using frequency locking to the vortex motion, we utilized a single LO source (100 GHz) with a test signal varying in a broad spectral range, 200–1400 GHz (see supplementary material Note 1 for more details). Although focusing on a more specific THz range would allow for a thorough performance optimization, we attempt to obtain a general understanding of the device operation as a coherent THz detector. In particular, we focused on both reaching high THz frequencies and high harmonic orders. Previous studies on both YBCO JJs[11,13,51] and equivalent Schottky diode[56] harmonic mixers indicate a reduction of

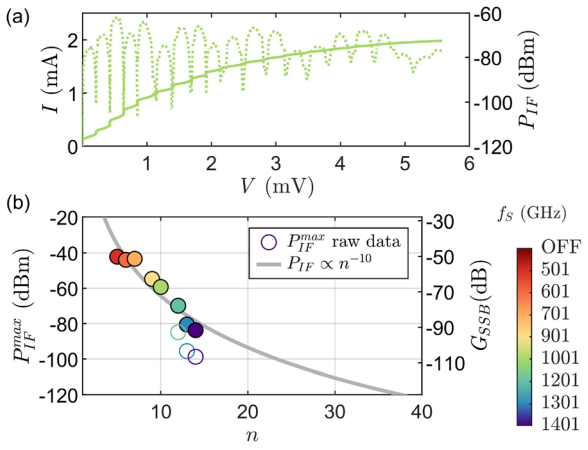

FIG. 5. Detection limit of the nanobridges at 59–58 K. (a) For the nanobridge with a cross section of 200×50 nm^2, both 100 GHz current steps (left axis) and harmonic mixing with 1.001 THz, i.e., the tenth harmonic (right axis), extend up to the flux-flow instability voltage (5.5 mV). (b) For the nanobridge with a cross section 70×50 nm^2, filled circles show the maximum intermediate frequency output power (left axis) and single sideband conversion efficiency G_{SSB} (right axis) as a function of the harmonic number n (filled circles) for a constant LO frequency (100 GHz). Open circles correspond to raw P_{IF}^{max} data measured at lower THz source power in the 1.1–1.5 THz range (x12, x13, x14 harmonics). These values were corrected by 15 dB (x30) to allow direct comparison with G_{SSB}, see details in supplementary material Note 6. The solid line is a $P_{IF} \propto n^{-10}$ fit. The y-axis is limited to −120 dBm, which corresponds to our noise threshold.

the mixing efficiency as the order of the harmonic increases. This trend is described by the empirical power law $P_{IF} \propto n^{\alpha}$ that reflects on the conversion efficiency $\eta = P_{IF}/P_{RF}$. While prior studies typically evaluated this decay by varying f_{LO} at a fixed signal frequency f_S, our methodology maintains a constant f_{LO} and varies f_S to track the harmonic response. From our measurements, we extract the averaged P_{IF}^{max}, which is plotted against the harmonic number n, correcting the source power variations at higher harmonics indicated with open circles in Fig. 5(b). This correction, takes into account the use of different sources and can be validated by the calculation of the single sideband conversion efficiency G_{SSB}, shown in Fig. 5(b) (see supplementary material Note 6). The resulting decay yields $\alpha = -10$. This value is an overestimation as increasing THz signal frequency increases losses in the YBCO-spiral antenna (including variation of its elliptical polarization), optical coupling loss, etc. However, with the current device, extrapolation based on our setup suggests a detection limit of up to 3.5 THz [see Fig. 5(b)].

Therefore, at this stage, the presented devices already demonstrate performance levels suitable for many practical applications, such as spectroscopy[57,58] or wireless communication.[59] Moreover, beyond their current technical capabilities, these devices offer a promising platform for exploring vortex dynamics potentially approaching the superconducting gap frequency.

See the supplementary material for detailed methods on thin-film growth, device fabrication, and the measurement setup. It also provides supporting data on the characterization of nanobridges, MATLAB simulations based on the RSJ model used to compare the datasets, and COMSOL simulations of hotspot formation in the nanobridges. In addition, it includes second-harmonic mixing measurements on a microbridge and an extended methodology describing the impact of variations in the incident THz source and the resulting conversion efficiency.

We acknowledge support by the Swedish Research Council (VR), under Project Nos. 2022-04334 (F.L.), 2020-05184 (T.B), and 2024-05138 (S.C.). We also acknowledge support from the Swedish infrastructure for micro- and nanofabrication—MyFab, Area of Advance Nano and Information and Communication programs at Chalmers University of Technology.

AUTHOR DECLARATIONS

Conflict of Interest

The authors have no conflicts to disclose.

Author Contributions

Núria Alcalde-Herraiz: Conceptualization (supporting); Formal analysis (equal); Investigation (supporting); Resources (equal); Visualization (equal); Writing – original draft (equal); Writing – review & editing (equal). **Alessia Garibaldi:** Resources (supporting); Writing – review & editing (supporting). **Karn Rongrueangkul:** Resources (supporting); Writing – review & editing (supporting). **Alexei Kalaboukhov:** Resources (supporting); Supervision (supporting); Writing – review & editing (supporting). **Floriana Lombardi:** Conceptualization (equal); Funding acquisition (equal); Supervision (equal); Writing – review & editing (equal). **Sergey Cherednichenko:** Conceptualization (equal); Funding acquisition (supporting); Investigation (equal); Writing – review & editing (equal). **Thilo Bauch:** Conceptualization (equal); Funding acquisition (equal); Supervision (lead); Writing – original draft (supporting); Writing – review & editing (equal).

DATA AVAILABILITY

The data that support the findings of this study are available from the corresponding author upon reasonable request.

REFERENCES

[1]M. K. A. Rogalski and P. Martyniuk, "Two-dimensional infrared and terahertz detectors: Outlook and status," Appl. Phys. Rev. **6**, 021316 (2019).
[2]R. Lewis, "A review of terahertz detectors," J. Phys. D **52**, 433001 (2019).
[3]Q. Qiu and Z. Huang, "Photodetectors of 2D materials from ultraviolet to terahertz waves," Adv. Mater. **33**, 2008126 (2021).
[4]X. Li, J. Li, Y. Li, A. Ozcan, and M. Jarrahi, "High-throughput terahertz imaging: Progress and challenges," Light. Sci. Appl. **12**, 233 (2023).
[5]P. H. Siegel, "Terahertz technology," IEEE Trans. Microwave Theory Tech. **50**, 910 (2002).
[6]J. Zmuidzinas and P. L. Richards, "Superconducting detectors and mixers for millimeter and submillimeter astrophysics," Proc. IEEE **92**, 1597 (2004).
[7]P. K. Day, H. G. LeDuc, B. A. Mazin, A. Vayonakis, and J. Zmuidzinas, "A broadband superconducting detector suitable for use in large arrays," Nature **425**, 817 (2003).
[8]J. Baselmans, F. Facchin, A. P. Laguna, J. Bueno, D. Thoen, V. Murugesan, N. Llombart, and P. De Visser, "Ultra-sensitive THz microwave kinetic inductance detectors for future space telescopes," Astron. Astrophys. **665**, A17 (2022).
[9]E. Novoselov and S. Cherednichenko, "Low noise terahertz MgB_2 hot-electron bolometer mixers with an 11 GHz bandwidth," Appl. Phys. Lett. **110**, 032601 (2017).
[10]E. B. I. Charaev, S. Cherednichenko, K. Reidy, V. Drakinskiy, Y. Yu, S. Lara-Avila, J. Thomsen, M. Colangelo, F. Incalza, K. Ilin, A. Schilling, and K. Berggren, "Single-photon detection using large-scale high-temperature MgB_2 sensors at 20 K," Nat. Commun. **15**, 3973 (2024).
[11]J. Chen, H. Myoren, K. Nakajima, and T. Yamashita, "THz mixing properties of $YBa_2Cu_3O_{7-x}$ grain boundary Josephson junctions on bicrystal substrates," Phys. C: Supercond. Appl. **293**, 288 (1997).
[12]M. Tarasov, E. Stepantsov, D. Golubev, Z. G. Ivanov, T. Claeson, O. Harnack, M. Darula, S. Beuven, and H. Kohlstedt, "Submillimeter-wave mixing and noise in high-temperature Josephson junctions," IEEE Trans. Appl. Supercond. **9**, 3761 (1999).
[13]Y. Fukumoto, R. Ogawa, and Y. Kawate, "Millimeter-wave detection by YBaCuO step-edge microbridge Josephson junction," J. Appl. Phys. **74**, 3567 (1993).
[14]X. Gao, J. Du, T. Zhang, Y. J. Guo, and C. Foley, "Experimental investigation of a broadband high-temperature superconducting terahertz mixer operating at temperatures between 40 and 77 K," J. Infrared, Millimeter, Terahertz Waves **38**, 1357 (2017).
[15]M. Malnou, A. Luo, T. Wolf, Y. Wang, C. Feuillet-Palma, C. Ulysse, G. Faini, P. Febvre, M. Sirena, J. Lesueur, and N. Bergeal, "Toward terahertz heterodyne detection with superconducting Josephson junctions," Appl. Phys. Lett. **101**, 233505 (2012).
[16]M. Malnou, C. Feuillet-Palma, C. Ulysse, G. Faini, P. Febvre, M. Sirena, L. Olanier, J. Lesueur, and N. Bergeal, "High-Tc superconducting Josephson mixers for terahertz heterodyne detections," J. Appl. Phys. **7**, 074505 (2014).
[17]J. Du, X. Gao, T. Zhang, and H. Zhu, "High-Tc superconducting quantum devices for cutting-edge terahertz technology," J. Phys. D **58**, 313001 (2025).
[18]H. Wang, Y. Aruga, T. Tachiki, Y. Mizugaki, J. Chen, K. Nakajima, T. Yamashita, and P. Wu, "Harmonic frequency mixing in $Bi_2Sr_2CaCu_2O_{8+x}$ intrinsic Josephson junctions," Appl. Phys. Lett. **75**, 2310 (1999).
[19]H. Wang, T. Tachiki, Y. Aruga, Y. Mizugaki, J. Chen, K. Nakajima, T. Yamashita, and P. Wu, "Microwave responses of BSCCO-2212 intrinsic

Josephson junctions at frequencies up to 100 GHz," in *Advances in Superconductivity XII: Proceedings of the 12th International Symposium on Superconductivity (ISS'99)* (Springer, 2000).
[20]H. Wang, L. You, J. Chen, P. Wu, and T. Yamashita, "Observation of Shapiro steps and spectroscopic applications of stacked intrinsic Josephson junctions up to the terahertz region," Supercond. Sci. Technol. **15**, 90 (2002).
[21]R. Vijay, J. Sau, M. L. Cohen, and I. Siddiqi, "Optimizing anharmonicity in nanoscale weak link Josephson junction oscillators," Phys. Rev. Lett. **103**, 087003 (2009).
[22]D. Rieger, S. Günzler, M. Spiecker, P. Paluch, P. Winkel, L. Hahn, J. Hohmann, A. Bacher, W. Wernsdorfer, and I. Pop, "Granular aluminium nanojunction fluxonium qubit," Nat. Mater. **22**, 194 (2023).
[23]P. Anderson and A. Dayem, "Radio-frequency effects in superconducting thin film bridges," Phys. Rev. Lett. **13**(6), 195 (1964).
[24]K. Likharev, "Superconducting weak links," Rev. Mod. Phys. **51**(1), 101 (1979).
[25]K. Likharev, "Vortex motion and the Josephson effect in superconducting thin bridges," Sov. Phys.-JETP **34**, 906 (1972).
[26]K. Xu and J. R. Heath, "Long, highly-ordered high-temperature superconductor nanowire arrays," Nano Lett. **8**, 3845 (2008).
[27]L. Embon, Y. Anahory, ŽL. Jelić, E. O. Lachman, Y. Myasoedov, M. E. Huber, G. P. Mikitik, A. V. Silhanek, M. V. Milošević, A. Gurevich, and E. Zeldov, "Imaging of super-fast dynamics and flow instabilities of superconducting vortices," Nat. Commun. **8**, 85 (2017).
[28]A. Llordes, A. Palau, J. Gázquez, M. Coll, R. Vlad, A. Pomar, J. Arbiol, R. Guzman, S. Ye, V. Rouco, F. Sandiumenge, S. Ricard, T. Puig, M. Varela, D. Chateigner, V. Moschalkov, G. Deutscher, C. Magen, and X. Obradors, "Nanoscale strain-induced pair suppression as a vortex-pinning mechanism in high-temperature superconductors," Nat. Mater. **11**, 329 (2012).
[29]O. Dobrovolskiy, D. Y. Vodolazov, F. Porrati, R. Sachser, V. Bevz, M. Y. Mikhailov, A. Chumak, and M. Huth, "Ultra-fast vortex motion in a direct-write Nb-C superconductor," Nat. Commun. **11**, 3291 (2020).
[30]T. Jalabert, E. Driessen, F. Gustavo, J. Thomassin, F. Levy-Bertrand, and C. Chapelier, "Thermalization and dynamics of high-energy quasiparticles in a superconducting nanowire," Nat. Phys. **19**, 956 (2023).
[31]E. Trabaldo, C. Pfeiffer, E. Andersson, R. Arpaia, A. Kalaboukhov, D. Winkler, F. Lombardi, and T. Bauch, "Grooved Dayem nanobridges as building blocks of high-performance $YBa_2Cu_3O_{7-\delta}$ SQUID magnetometers," Nano Lett. **19**, 1902 (2019).
[32]H. Rijckaert, P. Cayado, R. Nast, J. Diez Sierra, M. Erbe, P. López Dominguez, J. Hänisch, K. D. Buysser, B. Holzapfel, and I. Van Driessche, "Superconducting $HfO_2 - YBa_2Cu_3O_7$ nanocomposite films deposited using ink-jet printing of colloidal solutions," Coatings **10**, 17 (2019).
[33]M. F. Ritter, A. Fuhrer, D. Z. Haxell, S. Hart, P. Gumann, H. Riel, and F. Nichele, "A superconducting switch actuated by injection of high-energy electrons," Nat. Commun. **12**, 1266 (2021).
[34]M. Rocci, D. Suri, A. Kamra, G. Vilela, Y. Takamura, N. M. Nemes, J. L. Martinez, M. G. Hernandez, and J. S. Moodera, "Large enhancement of critical current in superconducting devices by gate voltage," Nano Lett. **21**, 216 (2021).
[35]R. Arpaia, E. Andersson, A. Kalaboukhov, E. Schröder, E. Trabaldo, R. Ciancio, G. Dražić, P. Orgiani, T. Bauch, and F. Lombardi, "Untwinned $YBa_2Cu_3O_{7-\delta}$ thin films on MgO substrates: A platform to study strain effects on the local orders in cuprates," Phys. Rev. Mater. **3**, 114804 (2019).
[36]R. Arpaia, E. Andersson, E. Trabaldo, T. Bauch, and F. Lombardi, "Probing the phase diagram of cuprates with $YBa_2Cu_3O_{7-\delta}$ thin films and nanowires," Phys. Rev. Mater. **2**, 024804 (2018).
[37]S. Nawaz, R. Arpaia, T. Bauch, and F. Lombardi, "Approaching theoretical depairing current in $YBa_2Cu_3O_{7-\delta}$ nanowires," Phys. C **495**, 33 (2013).
[38]R. Arpaia, D. Golubev, R. Baghdadi, R. Ciancio, G. Dražić, P. Orgiani, D. Montemurro, T. Bauch, and F. Lombardi, "Transport properties of ultrathin $YBa_2Cu_3O_{7-\delta}$ nanowires: A route to single-photon detection," Phys. Rev. B Condens. Matter. **96**, 064525 (2017).
[39]E. Trabaldo, "Noise and electrical properties of YBCO nanostructures," Ph.D. thesis (Chalmers University of Technology, Gothenburg, Sweden, 2020).
[40]E. Wahlberg, "Reshaping the phase diagram of $YBa_2Cu_3O_{7-\delta}$ through strain in ultrathin films and nanowires," Ph.D. thesis (Chalmers University of Technology, Gothenburg, Sweden, 2021).
[41]J. Bardeen, "Critical fields and currents in superconductors," Rev. Mod. Phys. **34**, 667 (1962).
[42]J. Schneider, H. Kohlstedt, and R. Wördenweber, "Nanobridges of optimized $YBa_2Cu_3O_{7-\delta}$ thin films for superconducting flux-flow type devices," Appl. Phys. Lett. **63**, 2426 (1993).
[43]W. Skocpol, M. Beasley, and M. Tinkham, "Self-heating hotspots in superconducting thin-film microbridges," J. Appl. Phys. **45**, 4054 (1974).
[44]G. Grimaldi, A. Leo, P. Sabatino, G. Carapella, A. Nigro, S. Pace, V. V. Moshchalkov, and A. Silhanek, "Speed limit to the Abrikosov lattice in mesoscopic superconductors," Phys. Rev. B **92**, 024513 (2015).
[45]H. Myoren, Y. Nishiyama, N. Miyamoto, Y. Osaka, and T. Hamasaki, "Josephson effect in wide superconducting bridges made by epitaxial $Ba_2YCu_3O_x$ thin films on YSZ/Si (100)," Jpn. J. Appl. Phys. **28**, L2213 (1989).
[46]S. Shapiro, "Josephson currents in superconducting tunneling: The effect of microwaves and other observations," Phys. Rev. Lett. **11**(2), 80 (1963).
[47]L. Aslamazov and A. Larkin, "Josephson effect in wide superconducting bridges," Zh. Eksp. Teor. Fiz **68**, 766 (1975).
[48]R. Baghdadi, R. Arpaia, T. Bauch, and F. Lombardi, "Toward $YBa_2Cu_3O_{7-\delta}$ nanoscale structures for hybrid devices," IEEE Trans. Appl. Supercond. **25**, 1 (2014).
[49]R. Arpaia, D. Golubev, R. Baghdadi, M. Arzeo, G. Kunakova, S. Charpentier, S. Nawaz, F. Lombardi, and T. Bauch, "Resistive state triggered by vortex entry in $YBa_2Cu_3O_{7-\delta}$ nanostructures," Phys. C: Supercond. Appl. **506**, 165 (2014).
[50]K. Lee, G. Park, L. Amatuni, and K. Constantinian, "Microwave properties of high-Tc $Y_1Ba_2Cu_3O_{7-y}$ superconducting bridges on Y_2BaCuO_5 substrates," J. Appl. Phys. **74**, 1448 (1993).
[51]J. Du, A. R. Weily, X. Gao, T. Zhang, C. P. Foley, and Y. J. Guo, "HTS step-edge Josephson junction terahertz harmonic mixer," Supercond. Sci. Technol. **30**, 024002 (2017).
[52]Y. Koval, M. V. Fistul, and A. V. Ustinov, "Incoherent microwave-induced resistive states of small Josephson junctions," J. Low Temp. Phys. **10**, 951–958 (2010).
[53]J. Wang, H. Li, E. Y. Cho, J. C. LeFebvre, K. Pratt, and S. A. Cybart, "Portable solid nitrogen cooling system for high transition temperature superconductive electronics," IEEE Trans. Appl. Supercond. **30**, 1–3 (2020).
[54]D. G. McDonald, A. Risley, J. Cupp, K. Evenson, and J. Ashley, "Four-hundredth-order harmonic mixing of microwave and infrared laser radiation using a Josephson junction and a maser," Appl. Phys. Lett. **20**, 296 (1972).
[55]A. I. Bezuglyj, V. A. Shklovskij, R. V. Vovk, V. M. Bevz, M. Huth, and O. V. Dobrovolskiy, "Local flux-flow instability in superconducting films near Tc," Phys. Rev. B **99**, 174518 (2019).
[56]D. Jayasankar, V. Drakinskiy, N. Rothbart, H. Richter, X. Lü, L. Schrottke, H. T. Grahn, M. Wienold, H.-W. Hübers, P. Sobis, and J. Stake, "A 3.5-THz, × 6-harmonic, single-ended Schottky diode mixer for frequency stabilization of quantum-cascade lasers," IEEE Trans. Terahertz Sci. Technol. **11**, 684 (2021).
[57]H. Bidgoli, S. Cherednichenko, J. Nordmark, H. Thunman, and M. Seemann, "Terahertz spectroscopy for real-time monitoring of water vapor and co levels in the producer gas from an industrial biomass gasifier," IEEE Trans. Terahertz Sci. Technol. **4**, 722 (2014).
[58]H. Richter, N. Rothbart, M. Wienold, X. Lü, K. Biermann, L. Schrottke, D. Jayasankar, J. Stake, P. Sobis, and H.-W. Hübers, "Phase locking of 3.5-THz and 4.7-THz quantum-cascade lasers using a Schottky diode harmonic mixer," IEEE Trans. Terahertz Sci. Technol. **14**, 346 (2024).
[59]J. Federici and L. Moeller, "Review of terahertz and subterahertz wireless communications," J. Appl. Phys. **107**, 111101 (2010).